

Large scale effects on the decay of rotating helical and non-helical turbulence

T Teitelbaum¹ and P D Mininni^{1,2}

¹ Departamento de Física, Facultad de Ciencias Exactas y Naturales, Universidad de Buenos Aires and CONICET, Ciudad Universitaria, 1428 Buenos Aires, Argentina.

² NCAR, P.O. Box 3000, Boulder, Colorado 80307-3000, U.S.A.

E-mail: teitelbaum@df.uba.ar

Abstract. Decaying three-dimensional (3D) turbulence is studied via direct numerical simulations (DNS) for an isotropic non-rotating flow and for rotating flows with and without helicity. We analyze the cases of moderate Rossby number and large Reynolds number focusing on the behavior of the energy spectrum at large scales and studying its effect on the time evolution of the energy and integral scales for $E(k) \sim k^4$ initial conditions. In the non-rotating case we observe the classical energy decay rate $t^{-10/7}$ and a growth of the integral length proportional to $t^{2/7}$ in agreement with the prediction obtained assuming conservation of the Loitsyanski integral. In the presence of rotation we observe a decoupling in the decay of the modes perpendicular to the rotation axis from the remaining 3D modes. These slow modes show a behavior similar to that found in two-dimensional (2D) turbulence whereas the 3D modes decay as in the isotropic case. We phenomenologically explain the decay considering integral conserved quantities that depend on the large scale anisotropic spectrum. The decoupling of modes is also observed for a flow with a net amount of helicity. In this case, the 3D modes decay as an isotropic fluid with a constant, constrained integral length, and the 2D modes decay as a constrained rotating fluid with maximum helicity.

1. Introduction

Controversy on the invariance of integral quantities in decaying turbulence has aroused during the last years [1]. Integral invariants are required to build phenomenological theories to explain the decay of kinetic energy and the evolution of integral length scales. For isotropic and homogeneous turbulence, the conservation of the Loitsyanski integral I for an initial spectrum $E(k \rightarrow 0) \sim Ik^4$ was called to derive the classical energy decay rate $E \sim t^{-10/7}$ and a growth of the integral length L proportional to $t^{2/7}$ [2]. In a similar fashion, for an initial spectrum $E(k \rightarrow 0) \sim Sk^2$, the assumed conservation of the integral quantity S associated to the conservation of linear momentum leads to $E \sim t^{-6/5}$ [3]. In practice, these quantities were shown to be only approximately conserved in closures [4] and in numerical simulations [5, 6] depending on the large scale spectrum of the initial conditions.

Less is known about the decay of turbulent flows in rotating reference frames. These flows have been largely studied due to its relevance for scientific and engineering problems. Their importance has motivated numerous theoretical, experimental, and numerical works. Applications are broad, including areas as diverse as turbo machinery and rotor-craft, convective region of the sun and stars, large-scale flows in oceans, and convective scales in the atmosphere.

It is well known that solid-body rotation inhibits the non-linear direct cascade of energy toward small scales reducing the dissipation rate of kinetic energy in comparison with non-rotating flows. This reduced dissipation has been observed in simulations [7, 8], experiments [9, 10], and studied theoretically [11]. An increase in the integral length parallel to the rotation axis with time has also been reported [12, 13] for these flows.

Resonant wave theory has been used to take into account the effect of rapid rotation in turbulence [14, 15, 16, 17]. According to this approach, the energy is transferred from small to large scales by resonant triadic interactions of inertial waves. The theory also argues that the resonant interactions are responsible for driving the flow to a quasi-two-dimensional state. In resemblance with the classic Taylor-Proudman theorem for steady flows [14], this result is often called the ‘‘Dynamic Taylor-Proudman Theorem’’ (see eg. [18]), and leads to the decoupling of slow modes which behave as an autonomous system of two-dimensional (2D) modes for the horizontal velocity components (perpendicular to the rotation axis) for strong rotation [16, 19].

As a result of this reduced non-linear coupling and dissipation, for decaying flows in the laboratory different scaling laws were observed as the flow decays [9, 20], from classical non-rotating values at small times changing to different power laws after a time of the order of $1/\Omega$. In [21], for example, an initial isotropic decay is observed, followed by a cross-over for $R_o \approx 0.25$ after which the energy decays slower ($E(t) \sim t^{-3/5}$). Such a decay law was proposed by [8] based on the assumption of energy transfer being governed by the linear time Ω^{-1} . Strong correlation of the vertical flow leading to the growth and subsequent saturation of the integral length by vertical confinement was observed

in [10, 12, 21]. This saturation was observed at a time proportional to $\Omega^{-5/7}$ in [10]. In [22] large-scale columnar-structure formation through linear inertial wave propagation was observed. Large scales form columnar eddies aligned with the rotation axis and a linear growth of the axial integral length takes place once the Rossby number passes below a certain threshold ($R_o \sim 0.4$). With the increase of rotation, energy is retained by stable large scale structures and prevented from cascading to small scales. In some cases, energy was observed to decay faster for larger rotation frequency.

In simulations, [23, 24] reported depletion of the nonlinear energy cascade and growth of anisotropy. Also, an increase on the energy decay rate with rotation frequency was observed for the isotropic as well as the perpendicular modes. Two-dimensionalization was reported in several works (see e.g., [25]), together with the formation of columnar structures [26] as seen in experiments. In [27], three distinct regimes were observed depending on the rotation frequency. At low rotation rates the flow behaves as non-rotating. At intermediate rotation rates, a strong coupling between rotation and non-linear interactions dominates (with a slower decay of the energy), and at high rotation rates viscous effects are dominant, damping the nonlinear effects. Recently, the cases of helical and non-helical rotating decaying turbulence with the integral scale of the size of the box were numerically studied in [28], where it was found that the presence of net helicity decreases even further the decay rate of energy (see also [29]). Rotating helicoidal flows have applications in atmospheric research, helical convective storms being an example [30].

To explain some of the experimental and numerical results, an extension to phenomenological predictions for rotating turbulence for $E(k \rightarrow 0) \sim Sk^2$ and $E(k \rightarrow 0) \sim Ik^4$ initial spectra (usually known as Saffman and Batchelor spectra respectively) has been proposed [8]. It includes a slow-down factor of the energy flux due to the presence of Rossby waves involving two different timescales: a long timescale representative of the turbulence evolution and a short one associated with the rotation frequency Ω . Conservation of S and I is then called to derive the asymptotic decay of energy for both initial spectra resulting in $E \sim t^{-3/5}$ and $E \sim t^{-5/7}$ respectively. In the case of constrained turbulence, phenomenology leads to $E \sim t^{-1}$. However, these phenomenological arguments do not consider the effect of anisotropies in the integral conserved quantities or in the decay laws.

In this work we numerically study the decay of rotating helical and non-helical turbulence with an emphasis on the anisotropies that arise when rotation is present, and on how integral quantities may be modified. The paper is divided in five sections. In section 2 we introduce the equations and describe how we solved them, with information regarding initial conditions. In section 3 we consider as an example a non-rotating flow, which behaves in agreement with previous results. In sections 4 and 5 we show and analyze results for the rotating non-helical and helical cases respectively. In the presence of rotation, we observe a decoupling of the energy decay rates for the 2D and three-dimensional (3D) modes. Studying the low wave number behavior we propose that the conservation of two-dimensional integral moments may explain these decays. In section

6 we finally summarize the results.

2. Numerical Simulations

The Navier-Stokes equation for an incompressible fluid in a rotating frame is solved numerically. When rotation is present, the equation reads

$$\partial_t \mathbf{u} + \boldsymbol{\omega} \times \mathbf{u} + 2\boldsymbol{\Omega} \times \mathbf{u} = -\nabla \mathcal{P} + \nu \nabla^2 \mathbf{u}, \quad (1)$$

together with the incompressibility condition

$$\nabla \cdot \mathbf{u} = 0. \quad (2)$$

Here \mathbf{u} is the velocity field, $\boldsymbol{\omega} = \nabla \times \mathbf{u}$ is the vorticity, $\mathcal{P} = p/\rho - (\boldsymbol{\Omega} \times \mathbf{r})^2/2 + \mathbf{u}^2/2$ is the total modified pressure, ρ is the (unit) density, and ν is the kinematic viscosity. We chose the rotation axis in the z direction so that $\boldsymbol{\Omega} = \Omega \hat{z}$, Ω being the rotation frequency. Our integration domain is a cubic box of length 2π with periodic boundary conditions and the equations were solved using a pseudo-spectral method with the 2/3-rule for de-aliasing. All runs were performed with a resolution of 512^3 grid points. The initial conditions were a superposition of Fourier modes with random phases and an energy spectrum $E(k) \sim k^4$ with modes randomly distributed in a spherical shell of wave numbers between 1 and 14. Details of the simulations are given in Table 1.

Table 1. Parameters used in the simulations: t^* refers to the time of maximum enstrophy; Re , R_o , R_o^w , H and h are respectively the Reynolds, Rossby, micro-Rossby numbers, the total helicity and the relative helicity. All quantities are calculated at time t^* . A resolution of 512^3 grid points was used in all runs.

Run	ν	Ω	Re	R_o	R_o^w	H	h	t^*
1	8.5×10^{-4}	0	420	—	—	0.01	1×10^{-4}	0.6
2	8.5×10^{-4}	10	450	0.1	0.95	0.05	4×10^{-3}	0.7
3	8.0×10^{-4}	10	530	0.07	0.7	6.5	0.5	1.5

In table 1, $Re = LU/\nu$ is the Reynolds number, $R_o^L = U/(2L\Omega)$ is the Rossby number based on the integral scale L , $R_o^w = w/(2\Omega)$ is the micro-Rossby number with $\omega = \langle \boldsymbol{\omega}^2 \rangle^{1/2}$, $H = \langle \mathbf{u} \cdot \boldsymbol{\omega} \rangle$ is the total helicity, $h = H/\langle |\mathbf{u}| |\boldsymbol{\omega}| \rangle$ is the relative helicity, and t^* is the time when maximum enstrophy is attained and when these quantities are measured. We use L defined as

$$L = 2\pi E^{-1} \int E(k) k^{-1} dk. \quad (3)$$

Note that R_o^w and R_o^L are one order of magnitude apart. This is required for rotation not to completely damp the non-linear term in the Navier-Stokes equation leading to a pure exponential decay (see [17] for more details).

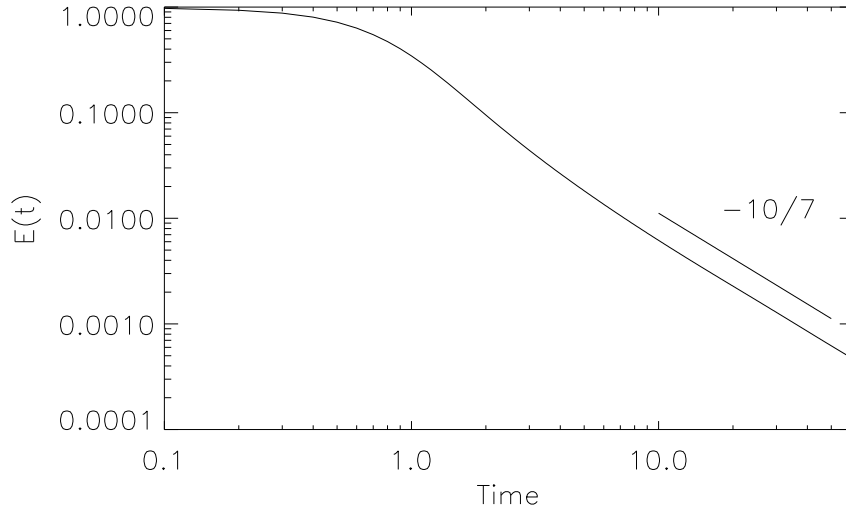


Figure 1. Energy decay for the non-rotating case (run 1). After a transient, the self-similar decay agrees with classical Kolmogorov theory. The $t^{-10/7}$ slope is shown as a reference.

3. Non-rotating flow

3.1. Phenomenological arguments

The classical Kolmogorov phenomenology leads to the well known energy spectrum

$$E(k) \sim \epsilon^{2/3} k^{-5/3}, \quad (4)$$

which for a decaying self-similar flow with $E(t) \sim kE(k)$ and using the balance equation $dE/dt \sim \epsilon$, gives the result

$$\frac{dE}{dt} \sim \frac{E^{3/2}}{L}. \quad (5)$$

L can depend on time and extra hypothesis are required to obtain the energy decay.

If $L \sim L_0$ (where L_0 is the size of the simulation domain), then $dE/dt \sim E^{3/2}/L_0$ and it follows that

$$E(t) \sim t^{-2}. \quad (6)$$

If $L \neq L_0$ but the spectrum at large scales is $\sim k^4$, conservation of an integral quantity can be assumed to derive the decay rate of this flow. Traditionally the conservation of an initial k^4 dependence in the low wave number spectrum $E(k)$ has been related to the invariance of the Loitsyanski integral I which we define as:

$$I = \int_0^\infty r^4 \langle \mathbf{u} \cdot \mathbf{u}' \rangle dr, \quad (7)$$

where $\langle \mathbf{u} \cdot \mathbf{u}' \rangle$ is the isotropic two-point longitudinal correlation function which depends solely on r . If conserved, from dimensional analysis it follows that $I \sim L^5 U^2$, then $dE/dt \sim E^{17/10}/I^{1/5}$ and we finally get

$$E(t) \sim t^{-10/7} \tag{8}$$

as obtained by Kolmogorov [2].

In practice, I evolves slowly in time and is only approximately conserved for an initial large scale spectrum $\sim k^4$. If the large scale spectrum is $\sim k^2$, then another integral quantity is approximately conserved [3], which leads to a decay $E(t) \sim t^{-6/5}$. In the next section we present a simulation (run 1 of table 1) which approximately follows the Kolmogorov decay (see also [5]). The rotating cases in section IV and V have the same large scale energy spectrum. Conditions where the integral length saturates (reaching the box size in numerical simulations) have been reported in [28].

3.2. Numerical results

In run 1 the energy spectrum (not shown) peaks initially at $k = 14$ and maintains an approximately k^4 scaling for low wave-numbers. The time history $E(t)$ for run 1 is shown in figure 1. After an initial transient of about six turn-over times, it shows a self-similar decay that is consistent with the $t^{-10/7}$ law.

In order to test further the behavior at large scales, we calculate the Loitsyansky integral I for this isotropic flow. In a recent work Ishida *et al.* estimated I by fitting $E = Ik^4/24\pi^2$ to the energy spectrum at large scales [5]. In their simulations (with spatial resolution of 1024 grid points and an initial peak of the spectrum near $k = 40$ or $k = 80$) the interval where $E \sim k^4$ holds is large enough for them to do the fitting. In our case (512 grid points) this interval is shorter and the fitting is not possible. Consequently, we checked spectral isotropy and then estimated I using equation (7). The two-point longitudinal correlation function can be estimated in the isotropic case using [1]:

$$\langle \mathbf{u} \cdot \mathbf{u}' \rangle(r) = 2 \int_0^\infty E(k)(\sin kr - kr \cos kr)/(kr)^3 dk, \tag{9}$$

where $E(k)$ is the isotropic energy spectrum.

The evolution of $I(t)/I(0)$ is shown in figure 3. Although $I(t)$ decays monotonically, after a transient its evolution is slow and it decreases only to approximately half its maximum value after 60 turn-over times. In [5] it was shown that its conservation improves as the extent of the large scale $\sim k^4$ spectrum is increased.

The approximate invariance of I can further be used to estimate the growth of L . Writing $L \sim I^{1/5}U^{-2/5}$ and replacing in equation (8) we get

$$L \sim t^{2/7}. \tag{10}$$

Figure 2 shows the evolution of the integral scale L_z based on the one-dimensional spectrum for run 1 calculated as:

$$L_z = 2\pi E^{-1} \int E(k_z)k_z^{-1} dk. \tag{11}$$

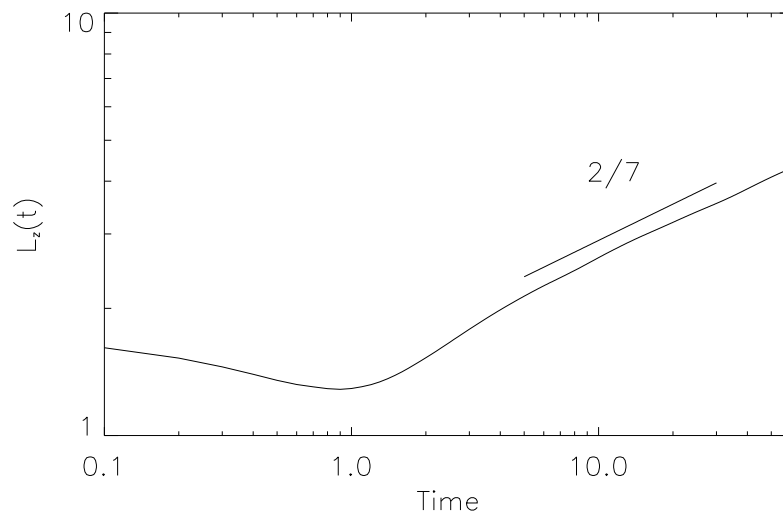


Figure 2. One-dimensional integral length scale L_z for run 1. After a transient period of time L_z grows approximately as $t^{2/7}$ as derived phenomenologically.

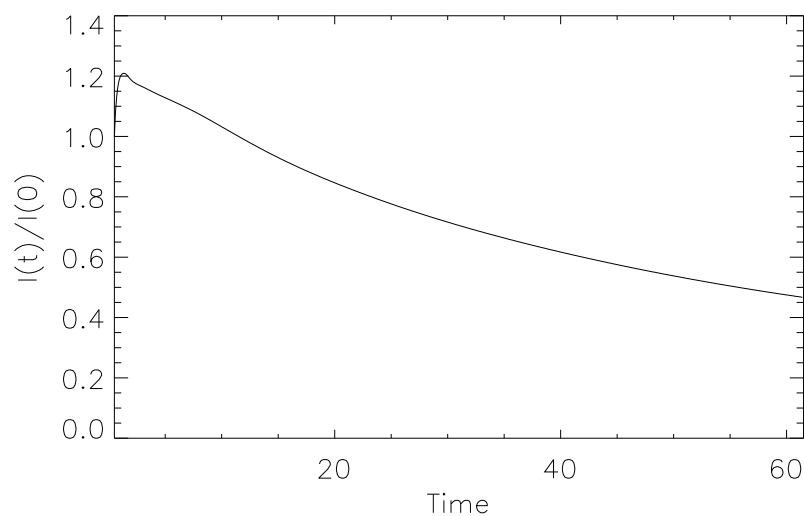


Figure 3. Normalized Loitsyansky integral I as a function of time for run 1.

After an initial transient L_z asymptotically settles down in the simulation to a growth rate close to $t^{2/7}$.

The results presented so far are consistent with Kolmogorov theory for decaying homogeneous and isotropic turbulence where initial conditions allow for the integral length to grow. In the next section we consider the analogy for the rotating case.

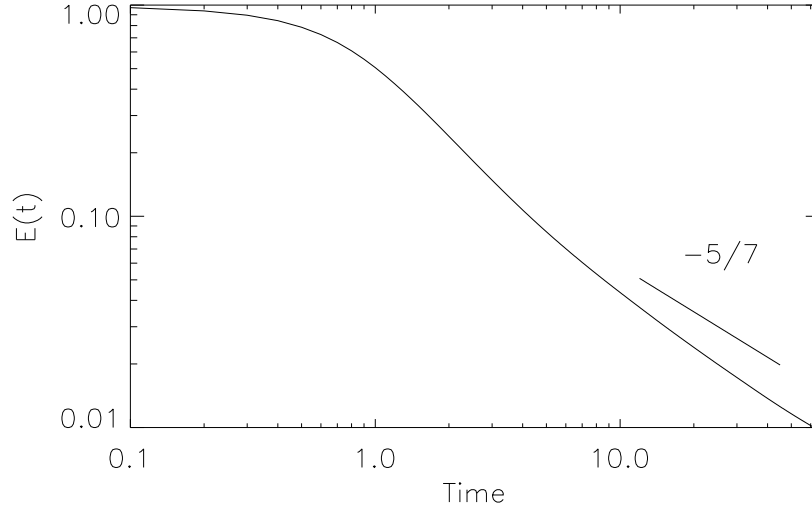


Figure 4. Energy as a function of time for run 2. After a transient, a decay close to although shallower than $t^{-5/7}$ is attained. A $t^{-5/7}$ slope is plotted for reference.

4. Rotating flow

4.1. Phenomenological arguments

In this section we analyze a flow subjected to solid-body rotation in the z axis with rotation frequency Ω (run 2). In non-helical rotating turbulence a

$$E(k) \sim \epsilon^{1/2} \Omega^{1/2} k^{-2} \quad (12)$$

spectrum is typically assumed [24, 31, 32, 33, 34]. From the balance equation this spectrum results in

$$dE/dt \sim (E/L)^2 1/\Omega. \quad (13)$$

Again, there are at least three possible scenarios. For $L \sim L_0$, $dE/dt \sim E^2$ [28] and

$$E(t) \sim t^{-1}. \quad (14)$$

When $L \neq L_0$ and $E(k) \sim k^4$ at large scales as in our runs, constancy of $I \sim U^2 L^5$ can be used again so that $dE/dt \sim E^{12/5}/(I^{2/5} \Omega)$ and [8]

$$E(t) \sim t^{-5/7}. \quad (15)$$

Invariance of I also leads to

$$L \sim t^{1/7}. \quad (16)$$

Finally, details of the rotating case with $E(k) \sim k^2$ can be found in [8].

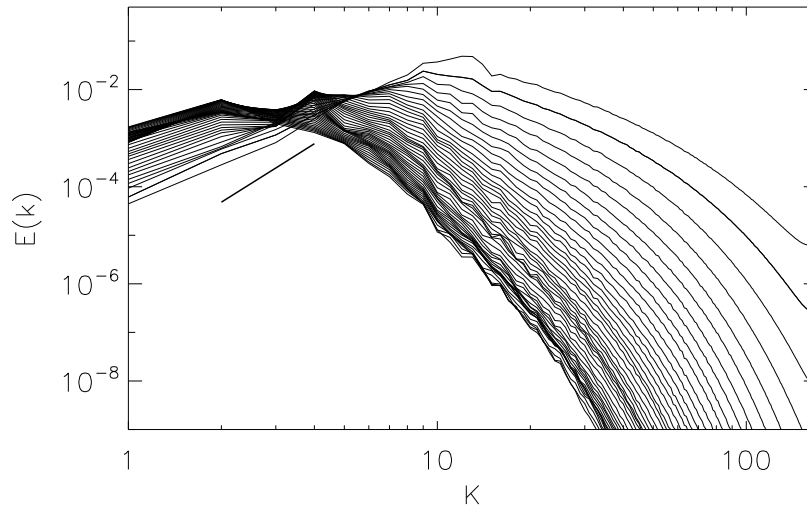


Figure 5. Energy spectrum $E(k,t)$ for run 2 from $t = 1$ to $t = 45$ in steps of $\Delta t = 1$. Energy piles up at large scales shallowing the spectra. A k^4 slope is shown for reference only.

4.2. Numerical results

Figure 4 shows the evolution of $E(t)$. After an initial nearly inviscid period, a transient period leads to a decay rate slightly steeper than $E \sim t^{-5/7}$.

The conservation of I assumed to derive $E(t) \sim t^{-5/7}$ is associated to a preserved k^4 spectrum at large scales. However, in the presence of rotation an inverse cascade of energy develops shallowing the spectrum at large scales as the energy piles up at low wave-numbers. This effect is visible in figure 5 where the isotropic energy spectra is plotted for different times. As a consequence I is no longer approximately conserved and varies fast. Figure 6 shows the evolution of $I(t)/I(0)$ departing from a constant value and increasing by an order of magnitude in clear contradiction with the hypothesis of constant I .

When rotation is present, isotropy breaks down, the flow becomes axisymmetric and a privileged direction (the z axis) exists. In figure 7 we show the evolution of the energy in the slow 2D modes of the velocity $E(k_{\parallel} = 0, t)$ (where $k_{\parallel} = k_z$ are the wave numbers in the direction parallel to the rotation axis), together with the energy of the remaining 3D modes with $E(k_{\parallel} \neq 0, t)$. The $k_{\parallel} \neq 0$ modes dominate initially having an amplitude one order of magnitude larger than the modes with $k_{\parallel} = 0$. This initial dominance is a result of the choice of initial conditions where Fourier modes are excited randomly all over shells in Fourier space, which results in most of the energy in modes with $k_{\parallel} \neq 0$.

As time evolves, energy from 3D modes is transferred to the $k_{\parallel} = 0$ plane and, after approximately six turn-over times, there is a cross-over after which energy in the 2D

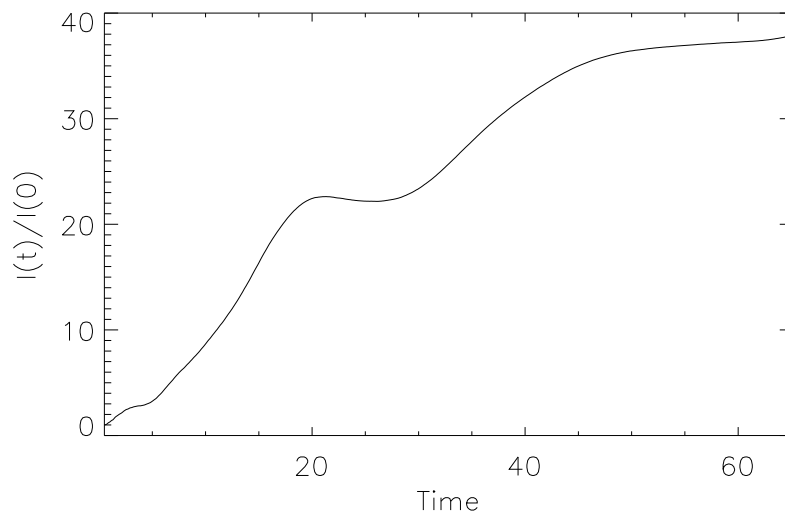


Figure 6. Isotropic Loitsyansky integral I for run 2

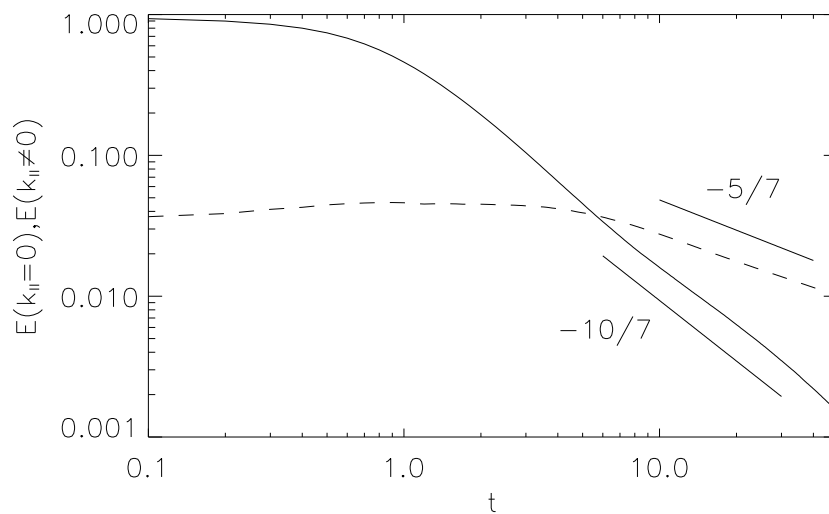


Figure 7. $E(t)$ for 3D modes with $k_{||} \neq 0$ (solid) and for 2D modes in the $k_{||} = 0$ plane (dashed) for run 2. Note an apparent decoupling in the decay rate between the energy in the 2D and the 3D modes.

modes prevails. Thereafter, 3D modes decay as in an isotropic flow without rotation following $E(k_{\parallel} \neq 0) \sim t^{-10/7}$ while perpendicular modes follow a shallower decay close to but now shallower than $E_{\perp} \sim t^{-5/7}$. This suggests that after $t \approx 6$ the evolution of the 2D and 3D modes decouple and they decay separately with their own decay rates. The Rossby Number at that time is $R_o \approx 0.015$, and the behavior is consistent with predictions of wave turbulence theory that obtains a decoupling for very small Rossby number [19, 18] with the 2D evolution of the modes described by the 2D Navier-Stokes equation.

4.3. Phenomenology revisited

This behavior naturally leads us to review two-dimensional integral moments in addition to the isotropic Loitsyansky integral already introduced. For two-dimensional turbulence, [6] and [35] suggest that three canonical cases exist: $E(k \rightarrow 0) \sim Jk^{-1}$, $E(k \rightarrow 0) \sim Kk$ and $E(k \rightarrow 0) \sim I_{2D}k^3$, where J , K and I_{2D} will be respectively defined here as

$$J = \int \langle \mathbf{w} \cdot \mathbf{w}' \rangle r dr, \quad (17)$$

$$K = \int \langle \mathbf{u} \cdot \mathbf{u}' \rangle r dr, \quad (18)$$

and

$$I_{2D} = \int r^3 \langle \mathbf{u} \cdot \mathbf{u}' \rangle dr. \quad (19)$$

Moreover, J and K are integral invariants of motion with conservation of K being associated with conservation of linear momentum and invariance of J a consequence of vorticity conservation. In the 3D rotating case, since the $k_{\parallel} = 0$ modes are the ones approximately decoupled for $R_o \ll 1$, and the equations for these modes are equivalent to the 2D Navier-Stokes equations [19, 18], we may wonder whether these integral quantities are conserved (or at least evolve slowly with time) in that manifold. In the rotating case, the relevant increments are then $r = r_{\perp}$ with \mathbf{r}_{\perp} perpendicular to $\boldsymbol{\Omega}$, and the associated wave vectors are \mathbf{k}_{\perp} .

We start by showing in figure 8 the energy spectrum for the vertically-averaged velocity field, that is to say, for wave numbers $k_{\perp}^2 = k_x^2 + k_y^2$ (hereafter, the perpendicular spectrum). This spectrum maintains a form proportional to k_{\perp}^3 (albeit slightly shallower).

In order to find slowly varying 2D-like integral quantities in the simulation, we calculate the time evolution of K and I_{2D} inverting the following equation which follows from assuming axisymmetry [1]:

$$E(k_{\perp}) = \int \frac{1}{2} \langle \mathbf{u} \cdot \mathbf{u}' \rangle k_{\perp} r_{\perp} J_0(k_{\perp} r_{\perp}) dr, \quad (20)$$

so that

$$\langle \mathbf{u} \cdot \mathbf{u}' \rangle(r_{\perp}) = \int 2E(k_{\perp}) J_0(k_{\perp} r_{\perp}) dk_{\perp} \quad (21)$$

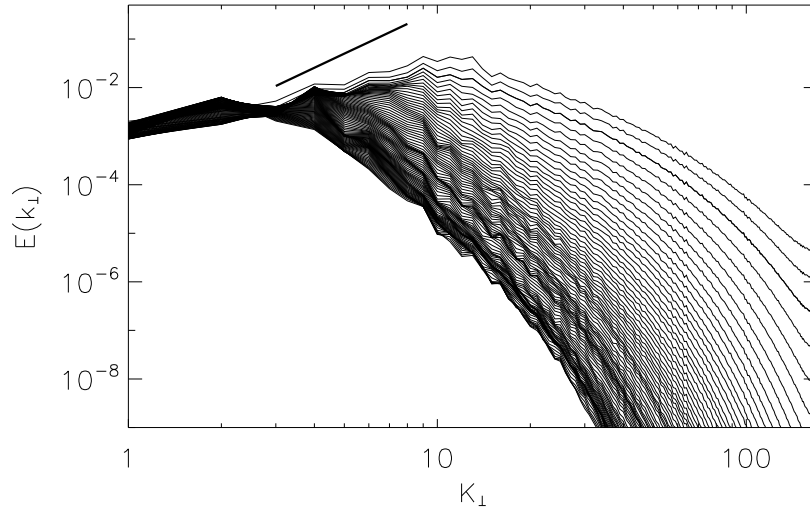


Figure 8. Evolution of the two-dimensional perpendicular spectrum $E(k_{\perp}, t)$ for run 2 from $t = 0.5$ to $t = 45$ in steps of $\Delta t = 0.5$. Note a slightly shallower than k^3 scaling for low wave numbers.

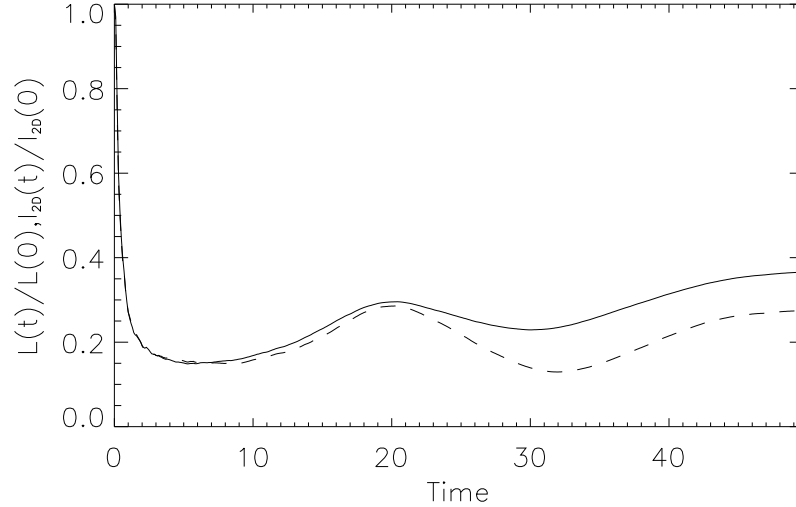


Figure 9. Normalized K (solid) and I_{2D} (dashed) as a function of time for run 2. Both parameters have a slow, almost constant behavior in time, showing little variation.

can be estimated from the perpendicular spectrum. The results for $K(t)/K(0)$ and $I_{2D}(t)/I_{2D}(0)$ are plotted in figure 9. Both magnitudes behave in a similar fashion, showing slow variations with a relative constant value over the simulated time.

Invariance of K or I_{2D} leads to different energy decay rates. For constant K we can write $K \sim L_{\perp}^2 U_{\perp}^2 L_{0\parallel}$ (where $L_{0\parallel}$ is the size of the box in the direction parallel to

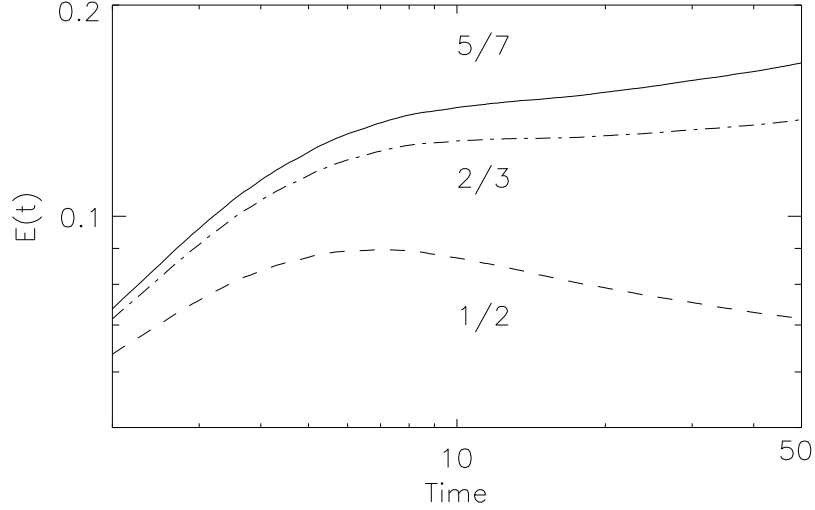


Figure 10. Energy decay for perpendicular ($k_{\parallel} = 0$) modes compensated by $t^{-\alpha}$ for $\alpha = 5/7$ (solid), $\alpha = 2/3$ (dot-dashed) and $\alpha = 1/2$ (dashed); $\alpha = 2/3$ adjusts our data better.

Ω) and assuming the slow-down factor in the energy dissipation rate by waves, as done in equation (13), $dE_{\perp}/dt \sim (E_{\perp}/L_{\perp})^2/\Omega$. Replacing L_{\perp} in the last equation we get $dE_{\perp}/dt \sim E_{\perp}^3 L_{0\parallel}/(K\Omega)$ leading to

$$E_{\perp} \sim t^{-1/2}. \quad (22)$$

For constancy of I_{2D} we have $I_{2D} \sim L_{\perp}^4 U_{\perp}^2 L_{0\parallel}$, and using the same arguments, from $dE_{\perp}/dt \sim (E_{\perp}/L_{\perp})^2/\Omega$ we get $dE_{\perp}/dt \sim E_{\perp}^{5/2} L_{0\parallel}^{1/2}/(I_{2D}^{1/2}\Omega)$, which finally leads to

$$E_{\perp} \sim t^{-2/3}. \quad (23)$$

In order to see whether any of these decay laws adjust our data better than the isotropic $\sim t^{-5/7}$ law, we plot the 2D energy evolution compensated by $t^{-5/7}$, $t^{-1/2}$, and $t^{-2/3}$ (figure 10). The decay law $E_{\perp} \sim t^{-2/3}$ seems to adjust better our simulation, which is consistent with the slow variation of I_{2D} and with the initial perpendicular spectrum close to k_{\perp}^3 .

The integral length parallel to the rotation axis $L_{\parallel} = L_z$ also behaves as in the isotropic case. In figure 11 we plot the evolution of L_{\parallel} compensated by the laws for the isotropic and axisymmetric cases already deduced. Clearly, the isotropic $t^{2/7}$ scaling adjusts better the results, in agreement with the isotropic-like decay of the energy in the 3D fast modes.

5. Helical Rotating Flow

We finally discuss briefly the effect of helicity upon the decay rate of energy in a rotating fluid. In order to incorporate net helicity into the flow we use a superposition of Arnold-

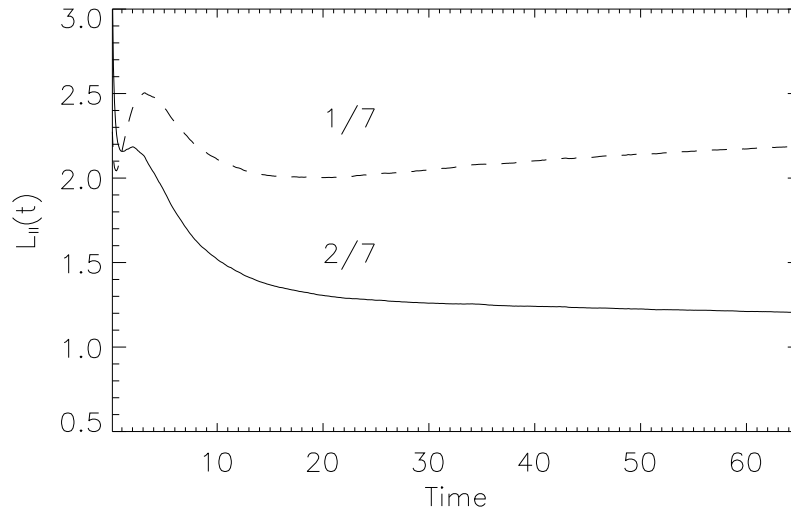


Figure 11. Integral length parallel to the rotation axis for run 2 compensated by $t^{-\alpha}$ for $\alpha = 2/7$ (solid) and $\alpha = 1/7$ (dashed); $t^{2/7}$ gives a better agreement to our data.

Beltrami-Childress (ABC) [36] initial conditions achieving an initial relative helicity $h \approx 0.99$. As in run 2, the ABC flows were added in all shells in Fourier space between wave numbers $k = 1$ to 14 with an isotropic spectrum $\sim k^4$.

Figure 12 shows a comparison between the energy as a function of time for the helical and non-helical rotating flows. The helical energy decay, shown in dashed line, is slower than the non-helical case. This retard has been associated with an inhibition of the non-linear transfer of the energy toward smaller scales by a direct cascade of helicity [40]. The behavior has also been observed in [28], where rotating helical and non-helical flows with constant integral length were studied.

The distinct evolution in the free decay of the helical flow can also be understood in terms of a phenomenological theory similar to those already presented. In this case, the direct transfer is dominated by the helicity cascade. Assuming maximal helicity we have [40]

$$E(k_{\perp}) \sim \epsilon^{1/4} \Omega^{5/4} k_{\perp}^{-5/2}. \quad (24)$$

Then it follows that

$$dE_{\perp}/dt \sim E_{\perp}^4 / (L_{\perp}^6 \Omega^5). \quad (25)$$

It is unclear at this point whether in the phenomenological analysis we should separate the decay of the 2D modes from the 3D modes as in run 2, and whether the integral scale changes in time or not. Therefore, in figure 13 we plot the 2D and 3D energy decays for run 3 (same as figure 7 but for the helical case). Note the anisotropic initial state with a relative excess of energy in the modes with $k_{\parallel} = 0$ due to the ABC initial conditions used. After the first nearly inviscid transient, both sets of modes seem

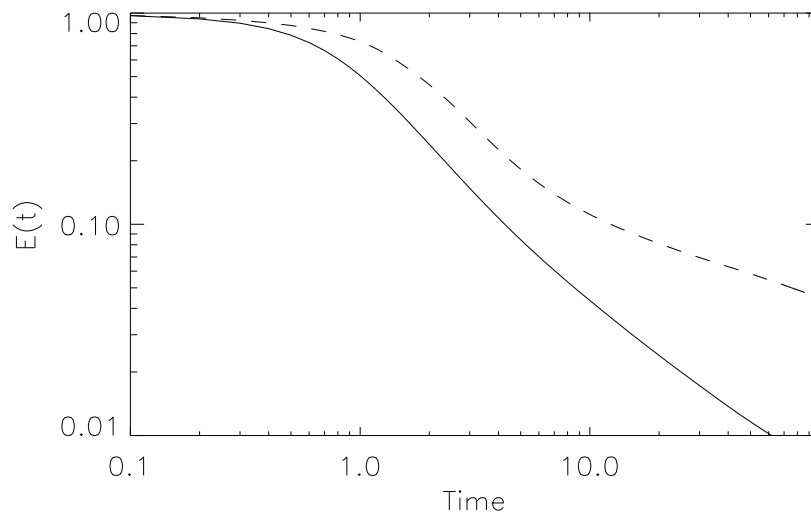


Figure 12. Total isotropic energy decay for helical (dashed) and non-helical (solid) rotating turbulence. The results show a decreased decay rate in the presence of helicity.

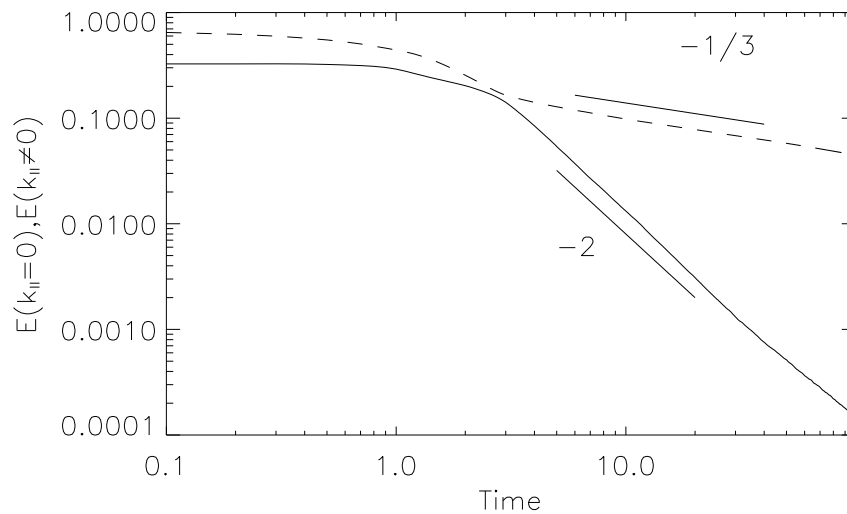


Figure 13. Decay of the energy for 3D modes with $k_{||} \neq 0$ (solid) and for 2D modes in the $k_{||} = 0$ plane (dashed) for the helical rotating flow (run 3) showing different scaling laws.

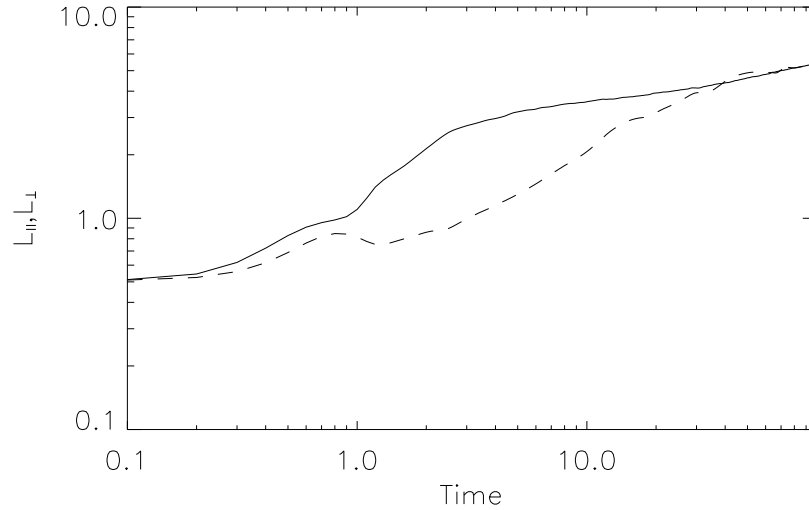


Figure 14. Integral length scales parallel (solid) and perpendicular (dashed) to the rotation axis as a function of time. Both lengths saturate fast to an almost constant value near the simulation domain length (2π).

again to decouple and decay with different laws: $\sim t^{-2}$ for the 3D modes and $\sim t^{-1/3}$ for the 2D modes. As in the non-helical case, the 3D modes decay faster, following the same law derived for an isotropic non-rotating flow where $L \sim L_0$. Indeed, in this run the integral scales grow fast during the transient and reach lengths close to the size of the box L_0 ($= 2\pi$) before the self-similar decay starts. This is illustrated in figure 14, that shows the evolution of the parallel and perpendicular integral scales. After $t \approx 6$ L_{\parallel} is almost saturated, and L_{\perp} keeps growing slowly but close to its maximum value. This results from a fast inverse transfer of energy (see the evolution of the isotropic energy spectrum in figure 15) that may be associated to the large amount of energy in the $k_{\parallel} = 0$ modes in the initial conditions.

The fast increase and saturation of L_{\parallel} and L_{\perp} give as a result the decay of the 2D and 3D modes as in constrained turbulence. For the 3D modes the $\sim t^{-2}$ decay then follows. For the 2D modes, using equation (25) and the approximate constancy of the integral lengths, we get a decay

$$E_{\perp} \sim t^{-1/3} \quad (26)$$

in agreement with the simulation. The study of the cases where the integral scales are not constant are left for future work, and may require the identification of anisotropic integral conserved quantities as in the previous section.

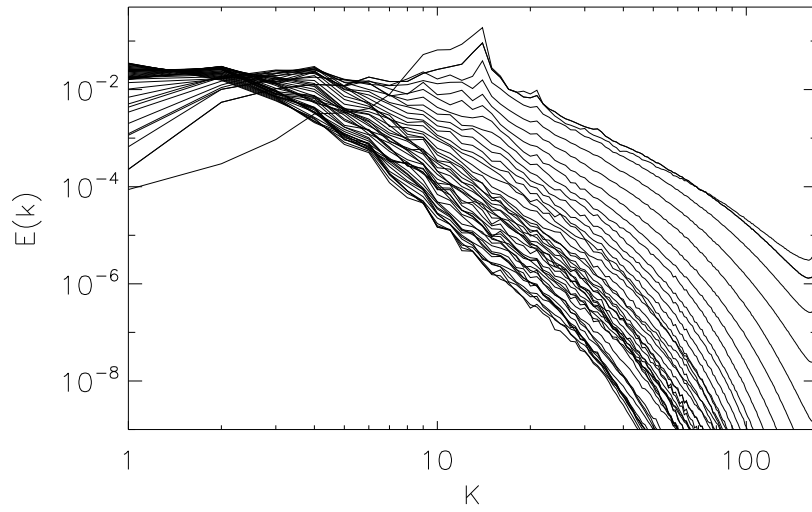


Figure 15. Isotropic energy spectrum $E(k,t)$ for run 3 from $t = 1$ to $t = 45$ in steps of $\Delta t = 1$.

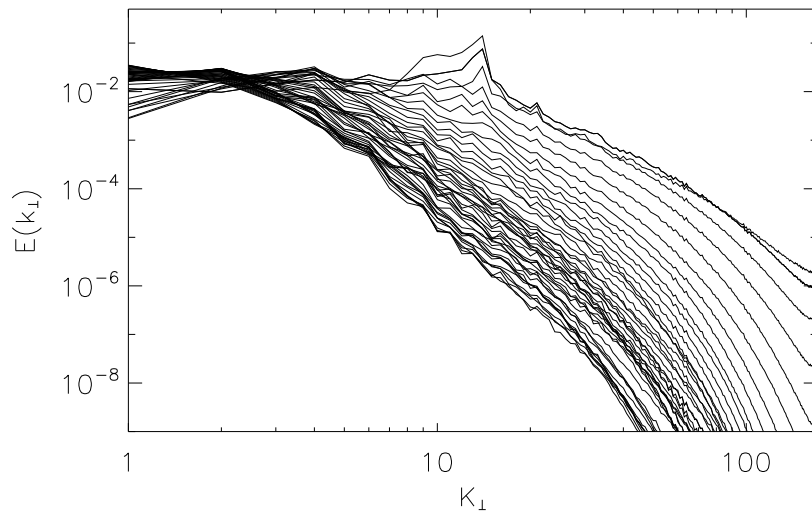


Figure 16. Perpendicular energy spectrum $E(k_{\perp},t)$ for run 3 from $t = 1$ to $t = 45$ in steps of $\Delta t = 1$.

6. Conclusion

In this work we presented studies of decaying turbulence in the presence of rotation and helicity. A simulation (run 1) without rotation and helicity was used to introduce some of the phenomenological arguments in unconstrained decaying turbulence. The simulation, with a large scale spectrum close to $\sim k^4$, shows a slowly varying Loitsyansky integral and a decay law consistent with Kolmogorov's $E(t) \sim t^{-10/7}$ law. Detailed studies of such a decay can be found in [5].

When extending these arguments to rotating turbulence, approximate conservation of isotropic integral moments (as e.g., the Loitsyansky integral) is often assumed (see e.g., [8]). A simulation of non-helical rotating turbulence (run 2) was shown to decay slightly faster than what is predicted by these arguments. We argued that the approximate decoupling of slow and fast modes predicted in wave turbulence theory for rotating flows at very small Rossby numbers leads to different decay laws for the energy in the 2D and 3D modes. The 3D modes decay in agreement with phenomenological predictions for isotropic and homogeneous turbulence, while the decay of the 2D modes is consistent with phenomenological results obtained assuming integral moments of the two-dimensional Navier-Stokes equation are approximately conserved.

Finally, the effect of helicity in rotating turbulence was considered in run 3. Helicity decreases the decay rate of turbulence even further as the direct transfer is dominated by the direct helicity flux (see e.g., [40, 28]), and helicity tends to decrease the amplitude of the non-linear term in the Navier-Stokes equation. The initial conditions considered led to the fast saturation of the integral scales, and as a result the 2D and 3D modes in this run decayed as constrained turbulence. The 3D modes decayed as in the non-rotating (constrained) case, while the 2D modes were observed to decay slower than what is predicted for constrained non-helical rotating turbulence and in agreement with predictions that consider the effect of helicity.

The three simulations presented here are far from an exhaustive exploration of the possible decay laws that may develop in rotating turbulence, and a detailed study of the effect of changing the initial large-scale energy spectrum dependence is left for future work, as well as studies of the effect of initial anisotropies in the decay, and the effect of scale separation between the initial integral scale and the box size (see e.g., [5] for a study for isotropic and homogeneous turbulence), and parametric studies varying the Reynolds and the Rossby numbers.

Acknowledgments

Computer time was provided by NCAR and CeCAR. The authors acknowledge support from grant UBACYT X468/08 and PICT 2007-02211. PDM is a member of the Carrera del Investigador Científico of CONICET.

References

- [1] Davidson P A 2004 *Turbulence: An introduction for scientists and engineers* (Oxford University Press)
- [2] Kolmogorov A N 1941 On the degeneration of isotropic turbulence in an incompressible viscous fluid *Dokl. Akad. Nauk SSSR* **31** 538-541
- [3] P G Saffman 1967 Note on decay of homogeneous turbulence *Phys. Fluids* **10** 1349
- [4] Herring J R, Kimura Y, James R, Clyne J, and Davidson P A 2005 Statistical and dynamical questions in stratified turbulence. In *Mathematical and Physical Theory of Turbulence* (ed. S. Shivamoggi) Taylor Francis
- [5] Ishida T, Davidson P A, and Kaneda Y 2006 On the decay of isotropic turbulence *J.Fluid Mech.* **564** 455-475
- [6] Davidson P A 2007 On the large-scale structure of homogeneous two-dimensional turbulence *J.Fluid Mech.* **580** 431-450
- [7] Mansour N N, Cambon C, and Speziale C G 1992 Theoretical and computational study of rotating isotropic turbulence, in *Studies in Turbulence*, edited by T.B Gatski, S.Sarkar and C.G. Speziale, (Springer-Verlag)
- [8] Squires K D, Chasnov J R, Mansour N N, and Cambon C 1994 The asymptotic state of rotating homogeneous turbulence at high Reynolds numbers, Application of direct and large eddy simulation to transition and turbulence” Chania, Crete, Greece
- [9] Morize C, Moisy F, and Rabaud M 2005 Decaying grid-generated turbulence in a rotating tank *Phys. Fluids* **17** 095105-095105-11
- [10] Morize C and Moisy F 2006 Energy decay of rotating turbulence with confinement effects *Phys. Fluids* **18** 065107-065107-9
- [11] Cambon C, Rubinstein R, and Godeferd F S 2004 Advances in wave turbulence: rapidly rotating flows *New J. Phys.* **6** 73
- [12] Bardina J, Ferziger J H, and Rogallo R S 1985 Effect of rotation on isotropic turbulence: computation and modeling *J. Fluid Mech.* **154** 321-336
- [13] Bartello P, Metais O, and Lesieur M 1994 Coherent structures in rotating three-dimensional turbulence *J. Fluid Mech.* **273** 1-29
- [14] Greenspan H P 1968 *The Theory of Rotating Fluids* (Cambridge University Press)
- [15] Greenspan H P 1969 On the nonlinear interaction of inertial waves *J. Fluid Mech.* **36** 257-286
- [16] Waleffe F 1993 Inertial transfers in the helical decomposition *Phys. Fluids A* **5** 677-685
- [17] Cambon C, Mansour N N, and Godeferd F S 1997 Energy transfer in rotating turbulence *J.Fluid Mech.* **337** 303-332
- [18] Chen Q, Chen S, Eyink G L, and Holm D D 2005 Resonant interactions in rotating homogeneous three-dimensional turbulence *J.Fluid Mech.* **542** 139-164
- [19] Majda A J and Embid P F 1998 Averaging over fast gravity waves for geophysics flows with unbalanced initial data *Theor. Comp. Fluid Dyn.* **11** 155-169
- [20] Seiwert J, Morize C, and Moisy F 2008 On the decrease of intermittency in decaying rotating turbulence *Phys. Fluids* **20** 071702-071702-4
- [21] Moisy F, Morize C, Rabaud M, and Sommera J 2009 Anisotropy and cyclone-anticyclone asymmetry in decaying rotating turbulence arXiv:0909.2599
- [22] Staplehurst P J, Davidson P A, and Dalziel S B 2008 Structure formation in homogeneous freely decaying rotating turbulence *J. Fluid Mech.* **598** 81-105
- [23] Thiele M and Muller W C 2009 Structure and decay of rotating homogeneous turbulence arXiv:0906.0853
- [24] Muller W C and Thiele M 2007 Scaling and energy transfer in rotating turbulence *Europhy. Lett.* **77** 3 34003-34003-5
- [25] Morinishi Y, Nakabayashi K, and Ren S Q 2001 Dynamics of anisotropy on decaying homogeneous turbulence subjected to system rotation *Phys. Fluids* **13** 2912-2922

- [26] Kuczaj A K, Geurts B J, and Holm D D 2009 Intermittency effects in rotating decaying turbulence arXiv:0904.0713
- [27] Yang X, Domaradzki J A 2004 Large eddy simulations of decaying rotating turbulence *Phys. Fluids* **16** 4088-4104
- [28] Teitelbaum T and Mininni P D 2009 Effect of helicity and rotation on the free decay of turbulent flows *Phys.Rev.Lett.* **103** 014501
- [29] Morinishi Y, Nakabayashi K, and Ren S 2001 Effects of helicity and system rotation on decaying homogeneous turbulence *JSME Int. J. Ser. B* **44** 410-418
- [30] Lilly D K 1986 The structure, energetics and propagation of convective rotating storms. Part II:Helicity and storm stabilization *atm. sc.* **43** 126-140
- [31] Bellet F, Godeferd F S, Scott J F, and Cambon C 2006 Wave turbulence in rapidly rotating flows *J.Fluid Mech.* **562** 83-121
- [32] Mininni P D, Alexakis A, and Pouquet A 2009 Scale interactions and scaling laws in rotating flows at moderate Rossby numbers and large Reynolds numbers *Phys. Fluids* **21** 015108
- [33] Zeman O 1994 A note on the spectra and decay of rotating homogeneous turbulence *Phys. Fluids* **6** 10 3221-3223
- [34] Zhou Y 1995 A phenomenological treatment of rotating turbulence *Phys. Fluids* **7** 2092-2094
- [35] Fox S and Davidson P A 2008 Integral invariants of two-dimensional and quasigeostrophic shallow-water turbulence *Phys. Fluids* **20** 075111
- [36] Childress S and Gilbert A D 1995 *Stretch, Twist, Fold: The fast dynamo* (Springer-Verlag Berlin)
- [37] Batchelor G K and Proudman I 1956 The large-scale structure of homogeneous turbulence *Phil. Trans. R. Soc. A* **248** 369-405
- [38] Ossia S and Lesieur M 2000 Energy backscatter in large-eddy simulations of three-dimensional incompressible isotropic turbulence *J.Turbulence* **1** 10(1)
- [39] Lesieur M and Ossia S 2000 3D isotropic turbulence at very high Reynolds numbers: EDQNM study *J. Turbulence* **1**(1) 7(1)
- [40] Mininni P D and Pouquet A 2009 Helicity cascades in rotating turbulence *Phys. Rev. E* **79** 026304